Conf-930749--52
BNL-49247
SSN-93-10

PROLIFERATION DETECTION USING A REMOTE RESONANCE RAMAN CHEMICAL SENSOR*

Arthur J. Sedlacek, Carl L. Chen and David R. Dougherty

Safeguards, Safety and Nonproliferation Division
Brookhaven National Laboratory
Building 197C
Upton, New York 11973

Introduction

Inseparable from any treaty or agreement is the need for verification. This verification can, and does, range from covert activities designed for detection of treaty non-compliance to overt, continuous on-site monitoring. However, as technology becomes available which can allow a party to easily engage in illicit behavior and help conceal this behavior, the need for detection technology that can flag the undesirable activities becomes an important corner stone for international security. With the break-up of the Former Soviet Union resulting in several of the new Commonwealth of Independent States (CIS) possessing weapons of mass destruction and with acquisition of nuclear, chemical and biological warfare capability by Third World countries, the urgency for detection/verification technology has never been greater. This new urgency is highlighted by the recent signing of the Chemical Weapons Convention (CWC) which goes far beyond the 24-year old Nuclear Nonproliferation Treaty (NPT) in many key respects, despite the fact that both are designed to help curtail the proliferation of weapons of mass destruction.[1] Similarly, especially with chemical and biological materials, the need for sensitive, accurate, fast, and portable detection technologies are urgently needed to undercover illicit activity whether it be chemical, nuclear or biological weapon development or drug manufacturing. Fortunately, state-of-the-art instrumentation is rapidly becoming available that can meet these widely varied needs and conduct the desired task at a high level of confidence, thus helping insure compliance with the relevant treaties.

Unfortunately, many technologies have varying detection and applicability characteristics which often dictate the conditions under which one can use the sensor to monitor, detect, identify or verify a chemical species.[2] In this report we will introduce the optical technique of resonance Raman spectroscopy for the remote detection, monitoring, identification and verification of proliferant effluents relevant to the production of weapons of mass destruction. A resonance Raman chemical sensor is an improvement on many technologies, save Fourier Transform Infrared spectroscopy (FTIR), in that optical fingerprints are at the heart of Raman spectroscopy. Fingerprinting has the obvious advantage that no prior knowledge is required of which chemicals are to be interrogated, as is *required* for both DOAS (differential optical absorption scattering) and DIAL (differential absorption LIDAR) (i.e., need to know the absorption maximum location so that one laser can be tuned to this maximum and the second detuned)[3] and because the optical signature *is* species specific. Furthermore, Raman scattering has the advantage that the spectral fingerprint is not obscured by water as is the case for both dispersive- and FT-infrared spectroscopy. Some of the other advantages[4-10] that a Raman sensor possesses are: (1) very high selectivity (chemical specific fingerprints), (2) independence from the excitation wavelength (ability to monitor in the solar blind region), (3) chemical mixture fingerprints are the sum of its individual components (no spectral cross-talk), (4) near independence of the Raman fingerprint to its physical state (very similar spectra for gas, liquid, solid and solutions), (5) no absolute calibration is necessary because all Raman signals observed from a given species can be compared with the Raman signal for N_2, whose concentration in the atmosphere is known very accurately, and (5) insensitivity of the Raman signature to environmental conditions (no quenching, or interference from water vapor). Resonance Raman spectroscopy can offer the fingerprinting advantage coupled with high sensitivity for trace analysis, providing a very powerful technique for detecting, identifying, monitoring, and, in the case of destruction, verifying many classes of chemicals.

Unfortunately, the inherently small scattering cross-sections for normal Raman scattering have effectively precluded the use of the technology outside of the lab. However, when the excitation frequency approaches an electronically excited state of the molecule[6,9,11-15], an enormous enhancement of the scattering cross-section can occur, often up to 4 to 6 orders of magnitude, and is referred to as resonance Raman (RR), since the excitation frequency is in "resonance" with an allowed electronic transition. This enhancement in the cross-section, in conjunction with the global advantages of Raman spectroscopy cited earlier, provide a promising optical open-path platform for the remote sensing of chemicals relevant of chemical weapons (CW) agent production as well as toxic chemicals and hazardous wastes. In addition, because water is

*This work was performed under the auspices of the U.S. Department of Energy, Contract No. DE-AC-02-76CH00016

a poor Raman scatterer, the measured Raman fingerprint is invariant to environmental perturbations. Furthermore, this scattering technique has equal applicability to gases, liquids, solids, and solutions.

Theory of Normal and Resonance Enhanced Raman Intensities

The fundamental equation which describes the Raman intensity[5,7,10,11] under *normal* scattering conditions is

$$I = K(\nu_o - \nu_{kl})^4 I_o \sum_{\rho\sigma} \left|(\alpha_{\rho\sigma})_{GF}\right|^2 \qquad (1)$$

where K is a constant, I_o is the incident light intensity (photons $sec^{-1}cm^{-2}$), ν_o is the frequency of the incident light wave, ν_{kl} is the vibrational frequency, and $(\alpha_{\rho\sigma})_{GF}$ is the transition polarizability tensor which, derived from second-order perturbation theory, is

$$(\alpha_{\rho\sigma})_{GF} = \frac{1}{\hbar}\sum_I \left(\frac{\langle F|\mu_\rho|I\rangle\langle I|\mu_\sigma|G\rangle}{\nu_{GI} - \nu_o + i\Gamma_I} + \frac{\langle I|\mu_\rho|G\rangle\langle F|\mu_\sigma|I\rangle}{\nu_{IF} + \nu_o + i\Gamma_I} \right) \qquad (2)$$

where the transition involves $|G\rangle$, $|F\rangle$, and $|I\rangle$, the initial, final and intermediate states, respectively, ρ and σ are the incident and scattered polarizations, Γ_I is a dampening factor reflecting the homogeneous width of state $|I\rangle$ and μ is the electron position operator. A very important result of Eqn. 2 is that as the laser frequency, ν_o, approaches the frequency of an allowed molecular transition, ν_{GI}, the denominator, $\nu_{GI} - \nu_o + i\Gamma_I$, becomes very small and the first term in the sum dominates, thereby making $(\alpha_{\rho\sigma})_{GF}$ very large: this is the ***resonance*** condition. It is important to understand that other factors, such as symmetry, add further requirements which mediate the strength of the resonance enhancement, but in principle, every molecule will have the resonance condition satisfied when excited with radiation whose energy is close to an electronic transition of the species.

Albrecht and Hutley[16] derived an expression for the polarizability having two major components such that the frequency dependence of the Raman intensity can be understood. The first term, corresponding to their A-term in the polarizability, has the following frequency dependence in scattering intensity

$$I \propto (\nu_o \pm \nu_{kl})^4 \left[\frac{\nu_e^2 + \nu_o^2}{(\nu_e^2 - \nu_o^2)^2} \right]^2 = F_A \qquad (3)$$

which is often referred to as the Franck-Condon factor term, where ν_e is the frequency of the resonant excited state . The A-term presupposes the existence of *one* electronic state being responsible for the resonance enhancement.

The second term of the polarizability tensor corresponds to Albrecht and Hutley's B-term which deals with a weakly allowed transition gaining intensity from a nearby strongly allowed transition. The frequency dependence of this term is described as

$$I \propto (\nu_o \pm \nu_{kl})^4 \left[\frac{\nu_e\nu_s + \nu_o^2}{(\nu_e^2 - \nu_o^2)(\nu_s^2 - \nu_o^2)} \right]^2 = F_B \qquad (4)$$

where ν_s is the frequency of the second electronic transition. In addition to being called the B-term, this term is also commonly referred as the Herzberg-Teller term.[5]

Under what conditions[2,5,6] does one term dominate? Generally speaking, the necessary conditions are reasonably well defined. When the transition matrix element is large and the excited-state potential function is shifted significantly from the ground-state equilibrium position and has a different shape, then the expected dominant factor is the Franck-Condon overlap (i.e., A-term); that is to say, there must be a large force-constant change associated with the excited state. Under these conditions, the relative intensities are governed by the overlap of vibrational states and consequently overtones can have significant intensity. Also, in order for the matrix element to be non-zero, it must be invariant to all symmetry operations of the molecular symmetry group, consequently, only totally symmetric vibrations will be enhanced. When the laser frequency is in resonance with a weakly allowed transition, significant enhancement can be observed if there is a nearby strongly allowed transition from which intensity may be borrowed. Under these circumstances, the second term will dominate because the Herzberg-Teller interaction will be larger than the Franck-Condon interaction. The major consequence of this term is that both non-totally symmetric and totally symmetric modes will undergo enhancement. This broad enhancement results because the intermediate state no longer needs to be totally symmetric. Finally, in the limit that an excited state's potential energy surface is similar to the ground state (i.e., little shift of the potential energy curve), the Franck-Condon overlap will result only in Rayleigh scattering. Under these conditions, the B-term is expected to dominate over

the A-term since the vibrational overlap will be very small.

Experimental Arrangement

The experimental configuration employed to collect the Raman signal from chemicals is typical of most experimental approaches. The output from an excimer laser (Lambda-Physik:LPX)-pumped dye laser (Lambda-Physik:LPD) is directed into a 2 mm x 2 mm quartz liquid cell (NSG Precision Cell Inc.). Frequency doubling of the dye-laser radiation is accomplished by nonlinear crystals (BBO 1). Both the Rayleigh and Raman scattering is collected in the 90° configuration by a double-grating SPEX (F/6.5, .75 meter) monochromator (2400 grooves/mm, blazed at 250 nm) and detected by a optical multichannel analyzer (EG&G 1471 blue-enhanced). If desired, the scattering arrangement can be quickly altered to a 180° backscattering configuration. The excitation beam is brought into the sample from below thus enabling more efficient coupling of the irradiated area into the spectrometer. Both the monochromator and optical multichannel analyzer (OMA) are interfaced to a Macintosh IIfx computer where the collected signals are stored for later analysis.

Results and Discussion

Figures 1a and 1b show the fingerprint region of cyclohexane following irradiation at 440 nm and 220 nm, respectively. Also shown, in the inset of figure 1a, is the ultraviolet absorption of cyclohexane. The striking feature between these two spectra is that the 802 cm^{-1} peak appears to grow weaker as the excitation is shifted to shorter wavelengths. Instead, however, the other modes of cyclohexane are undergoing a significant *pre-resonance* enhancement.

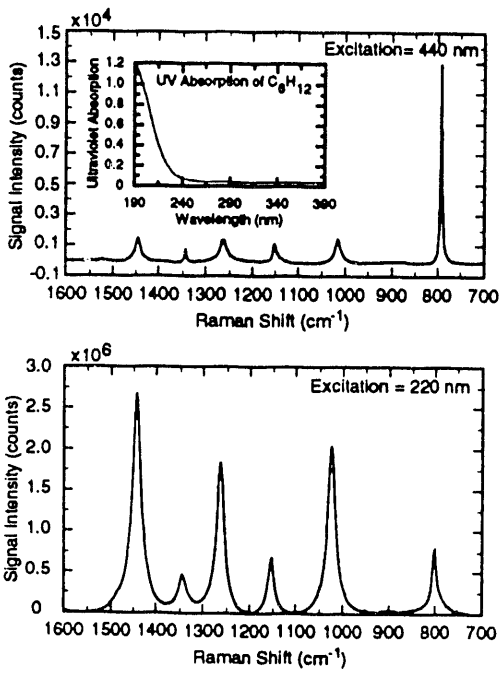

Figure 1

Following this initial finding, we then measured the differential Raman scattering cross-sections for the 802 cm^{-1} and 1028 cm^{-1} peaks as a function of excitation wavelength. In an effort to understand more completely the mechanism responsible for the observed enhancement, the cyclohexane data were fit to Albrecht's A-term and B-term[16] (Eqns. 3 and 4). However, fitting these 802 cm^{-1} data to Albrecht's B-term was unsuccessful. The 802 cm^{-1} data set was then fit to a modified version of the A-term in order to account for a frequency-independent contribution to the enhancement in accord with that suggested by Asher.[12] Plotted on the same graph in Figure 2a is the predicted ν^4-dependence of the Raman intensity. In the figures below, the solid circles represent the Raman scattering cross-sections measured in the present investigation and the open circles are data from other studies.[17-21]

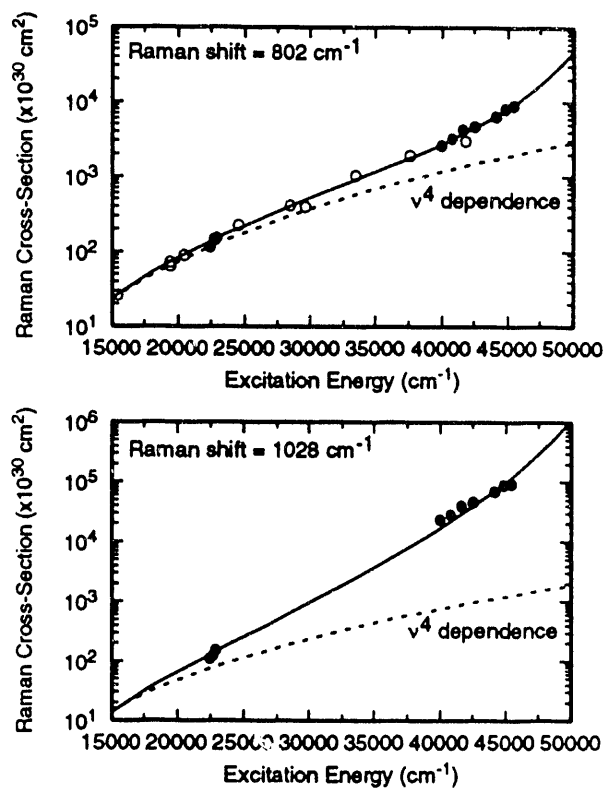

Figure 2

As is readily observable, the fit to the modified Albrecht A-term is quite good and shows how the enhancement becomes greater as the excitation energy approaches resonance with the allowed electronic transition. Since the modified A-term slightly underestimates the energy of the lowest electronic state and the original A-term slightly overestimates its value, the energy of the lowest electronic state that couples to this mode is taken as the average from these two extremes. The energy of the lowest electronically excited state that couples to the 802 cm^{-1} vibration is estimated to be ~82500

cm^{-1}. An examination of the vacuum ultraviolet (VUV) spectrum[22] of cyclohexane reveals that a strongly allowed σ-σ^* (CC) transition occurs between 75000 cm^{-1} and 95000 cm^{-1} and is probably responsible for the pre-resonance enhancement that is observed.

Since the data set for the 1028 cm^{-1} vibration was not nearly as complete as for the 802 cm^{-1} vibration, this mode was fit to only the A-term. As is clearly observed in Figure 2b, the curve fitting is at best marginal. This probably results from (1) too few data over the large range of excitation energies used in the fit and (2) the energy of the lowest electronic state that couples to this mode is predicted to be ~57700 cm^{-1} and therefore this mode is probably undergoing a resonance enhancement and the approximations used to derive the A-term are no longer valid. A transition centered around 63000 cm^{-1} is the most likely candidate responsible for this mode's enhancement. Fits to the other functional forms did not result in any significant improvement in the fit.

The resonance enhancement of acetonitrile[23] in the UV is even more impressive. Collected in Figure 3 is the C-H stretching region of CH_3CN as a function of 3 excitation wavelengths, 440, 225 and 220 nm. On the scale displayed for the 440 nm results, the ν_5 mode of CH_3CN at 3000 cm^{-1} is not even visible; however, at 225 nm it is of nearly equal intensity to the ν_1 mode at 2950 cm^{-1}, and a reduction of the excitation wavelength of only 5 nm results in a further dramatic enhancement of this mode. Calibration of the area under this transition to the 973 cm^{-1} mode reveals that the ν_5 mode undergoes an enhancement in excess of 10^6, resulting in a total resonance enhanced scattering cross-section of ~$1x10^{-23}$ cm^2.

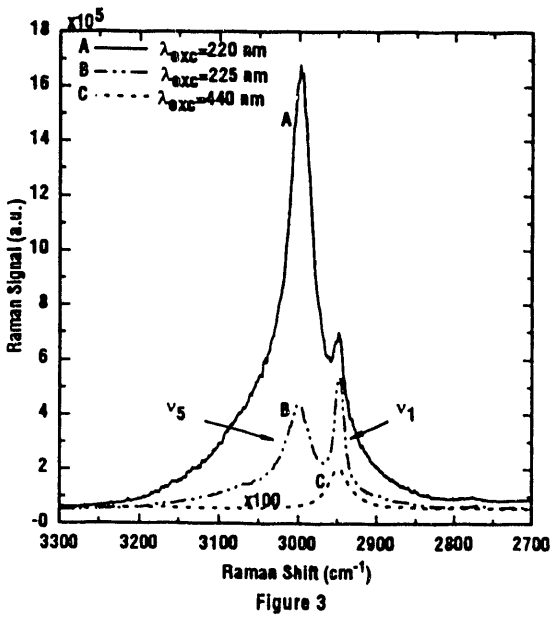

Figure 3

Although we have not yet mapped out this mode's resonance enhancement, several strong broad absorption features exist just below ~170 nm and represent the most likely transitions responsible for the huge enhancement. Current research effort is aimed at mapping out the frequency dependence of the scattering cross-section in order to obtain an estimate of the energy of the lowest electronic state that couples to this mode.

Remote Resonance Raman Chemical Sensor

The whole purpose of measuring the resonance Raman cross-sections is to estimate the potential for a remote resonance Raman chemical sensor. Since this phenomenon is inherently a scattering process, its extension to the remote detection of effluents should be straightforward with the only critical requirement being the size of the resonance Raman scattering cross-section. To properly evaluate the potential of this extension, we have examined the resonance Raman signal dependence under a variety of conditions using the following inelastic scattering return-signal equation,[2,24]

$$S = 2.69x10^5\,\eta N \frac{E}{\hbar\omega_o}\frac{AL}{R^2}\rho\frac{d\sigma}{d\Omega}\left[\exp -2(\alpha_s+\alpha_o)R\right] \quad (5)$$

where η is the total detection efficiency, N the number of excitation/probing pulses, E the laser pulse energy, ω_o the laser frequency, A the collector area (cm^2), L the range increment (m), R the range (km), and α_o and α_s the atmospheric absorption/aerosol scattering coefficients at the laser and scattering frequencies. The numerical factor out in front of the equation allows the concentration of the species, ρ, to be expressed in ppm and $d\sigma/d\Omega$ is the RR differential scattering cross-section. For the following assessment, we have assumed a 5% total collection efficiency at a laser wavelength of 266 nm (quadrupled Nd:YAG laser) at a repetition rate of 500 Hz, with a collector area of ~10^4 cm^2 and a visibility of 23 km. We evaluated Eqn. 5 under a signal-to-noise (S/N) ratio of 10 ($\sqrt{S}$). Other factors used are collected in Table I.[25]

Shown in Figure 4a is the sensitivity of a UVRR remote sensor as a function of both range and integration time. It can be seen that integrating scattered light for 60 seconds from a stack 1 km away with a differential cross-section of $7x10^{-25}$ cm^2/sr will allow detection of an effluent at the sub-ppm·m level. Alternatively, at a distance of 5 km, the effluent could be detected at the low ppm level. Even with an integration time as short as 10 seconds, ppm·m could easily be detected at a distance of 1 km. Displayed in Figure 4b is the RR remote chemical sensor sensitivity as a function of

both range and differential scattering cross-section. Here we can see that even when the differential cross-section is as small as 10^{-27} cm^2/sr and the laser pulse energy is as low as 10 mJ, the detection concentration, with 60 seconds integration time, is at the 100s ppm level. The ability to use laser excitation below 300 nm is significant because interrogation of a plume can be done during the day without necessary solar background corrections that would otherwise be required. Of course, care must be taken when working in the UV because of the strongly absorbing ozone.

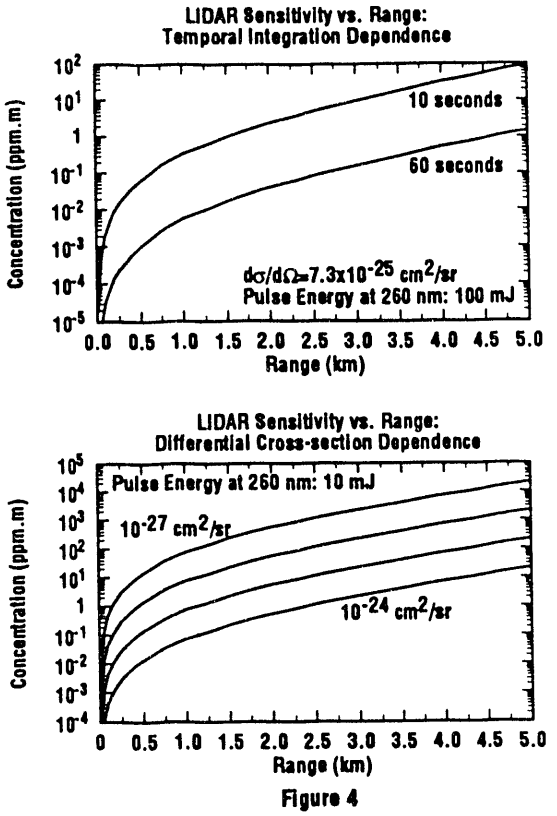

Figure 4

Melfi[26-27] of NASA and others[28-32] have employed a normal Raman chemical sensor system to probe/monitor water vapor in the atmosphere from ground level up to 13 km from a ground-based system. In Melfi's remote sensor system, a XeF excimer laser operating at 351 nm is employed and a series of bandpass filters are used to isolate spectral regions for water (3000-4000 cm^{-1}), O_2 and N_2. His success suggests that a resonance Raman-based remote sensor system should offer great potential, especially in light of the fact that the differential scattering cross-section for water is only ~10^{-29} cm^2/sr and the differential scattering cross-sections typically found for molecules with pre-resonance or resonance enhancement range from 10^{-26} cm^2/sr to 10^{-23} cm^2/sr. Further evidence is provided by the series of studies conducted by Hirschfeld et al.[33] in the early 1970s where the potential of normal Raman sensor was demonstrated by monitoring SO_2, CO_2, H_2O and kerosene emissions from a stack. In that project, a doubled ruby laser (λ_{exc}=347.15 nm) was employed along with the state-of-the-art photomultiplier tubes (PMT) and collection optics. Using a range resolution of 10 m, their instrument could measure the concentration of SO_2 at 30 ppm and kerosene at 1.7 ppm at a distance of 200 m with a 36 inch collection optic. These results were without the aid of resonance enhancement, which would lower the detection limits or increase the monitoring range.

Conclusions and Prognosis

We have discussed the potential of the resonance Raman chemical sensor as a remote sensor that can be used for gases, liquids or solids. This spectroscopy has the fundamental advantage that it is based on optical fingerprints that are insensitive to environmental perturbations or excitation frequency. By taking advantage of resonance enhancement, the inelastic scattering cross-section can increase anywhere from 4 to 6 orders of magnitude which translates into increased sensing range or lower detection limits. It was also shown that differential cross-sections as small as 10^{-27} cm^2/sr do not preclude the use of this technique as being an important component in one's remote-sensing arsenal. The results obtained in the early 1970s on various pollutants and the more recent work on atmospheric water cast a favorable light on the prospects for the successful development of a resonance Raman remote sensor. Currently, of the 20 CW agent-related "signature" chemicals that we have investigated, 18 show enhancements ranging from 3 to 6 orders of magnitude. The absolute magnitudes of the measured resonance enhanced Raman cross-sections for these 18 chemicals suggest that detection and identification of trace quantities of the "signature" chemicals, through a remote resonance Raman chemical sensor, could be achieved.

References:

1. M. Krepon, Arms Control Today, **October,** 19 (1992).
2. For example, see Grant, W. B., Kagann, R. H. and McClenny, W. A., J. Air Waste Manage. Assoc. **42**, 18 (1992).
3. Measures, R. M., Laser Remote Chemical Analysis, in *Chemical Analysis Series Vol. 94*, R. M. Measures, Ed., John Wiley and Sons: New York 1988.
4. Hendra, P., Jones, C. and Warnes, G., *Fourier Transform Raman Spectroscopy: Instrumentation and Chemical Applications*, Ellis Horwood: New York 1991.
5. Grasselli, J. G. and Bulkin, B. J., *Analytical Raman Spectroscopy*, John Wiley and Sons: New York 1991.

6. Carey, P. R., *Biochemical Applications of Raman and Resonance Raman Spectroscopies*, Academic Press: New York 1982.
7. Schrötter, H. W. and Klöckner, H. W., Raman Spectroscopy of Gases and Liquids in *Topics in Current Physics*, A. Weber, Ed., Springer-Verlag: New York 1979.
8. Long, D. A., *Raman Spectroscopy*, McGraw-Hill: New York 1977.
9. Nelson, W. H. and Sperry, J. F., *Modern Techniques for Rapid Microbiological Analysis*, W. H. Nelson, Ed., VCH Publishers: New York 1991.
10. Wilson Jr., E. B., Decius, J. C. and Cross, P. C., *Molecular Vibrations*, Dover Publications: New York 1955.
11. Rousseau, D. L., Friedman, J. M. and Williams, P. F., Raman Spectroscopy of Gases and Liquids, in *Topics in Current Physics*, A. Weber, Ed., Springer-Verlag: New York 1979.
12. Asher, S. A., Anal. Chem. **56**, 720 (1984).
13. Asher, S. A., *Ann. Rev. Phys. Chem.* **39**, 537 (1988).
14. Ziegler, L. D. and Albrecht, A. C., J. Chem. Phys. **70**, 2634 (1979).
15. Hirakawa, A. Y. and Tsuboi, M., Science **188**, 359 (1975).
16. Albrecht, A. C. and Hutley, M. C., J. Chem. Phys. **55**, 4438 (1971).
17. Trulson, M. O. and Mathies, R. A., J. Chem. Phys. **84**, 2068 (1986).
18. Colles, M. J. and Griffiths, J. E., J. Chem. Phys. **56**, 3384 (1972).
19. Murphy, W. F., Holzer, W. and Bernstein, H. J., Appl. Spectrosc. **23**, 211 (1969).
20. Abe, N., Wakayama, M. and Ito, M., J. Raman Spectrosc. **6**, 38 (1977).
21. Nestor, J. R. and Lippincott, E. R., J. Raman Spectrosc. **1**, 305 (1973).
22. Raymonda, J. W. and Simpson, W. T., J. Chem. Phys. **47**, 430 (1967).
23. Dudik, J. M., Johnson, C. R. and Asher, S. A., J. Chem. Phys. **82**, 1732 (1985).
24. Rosen, H., Robrish, P. and Chamberlain, O., Appl. Optics **14**, 2703 (1975).
25. Scattering data taken from "Optical Properties of the Atmosphere", AFCRL-72-0497, 24 August 1972.
26. Melfi, S. H., Appl. Optics **11**, 1605 (1972).
27. Melfi, S. H., Koutsandreas, J. D. and Moran, J., Environ. Sci. Technol. **11**, 36 (1977).
28. Bilbe, R. M., Bullman, S. J. and Swaffield, F., Meas. Sci. Technol. **1**, 495 (1990).
29. Riebesell, M., Voss, E., Lahmann, W., Weitkamp, C. and Michaelis, W., *Proc. Int. Conf. Lasers*, **1987**, 129.
30. Cooney, J., Petri, K. and Salik, A., Appl. Opt. **24**, 104 (1985).
31. Petri, K., Salik, A. and Cooney, J., Appl. Opt. **21**, 1212 (1982).
32. Renaut, D., Pourny, J. C. and Capitini, R., Opt. Lett. **5**, 233 (1980).
33. Hirschfeld, T., Schildraut, E. R., Tannenbaum, H. and Tanenbaum, D., Appl. Phys. Lett. **22**, 38 (1973).

TABLE I: Parameters Employed for Remote Resonance Raman Chemical Sensor Evaluation

Parameter	Value
Detection efficiency (η)	5%
Number of laser pulses (N)	rep. rate: 500 Hz
Laser pulse energy (E)	100 mJ
Laser frequency/wavelength (ω_O)	260 nm
Collector area (A)	~10^4 cm^2
Range increment (L)	4.5 m
Atmospheric abs. coeff. @ laser frequency (α_O)	0.3 km^{-1}
Atmospheric abs. coeff. @ scattered frequency (α_S)	0.3 km^{-1}

END

DATE
FILMED
10/7/93